MASS MOVEMENT POTENTIAL AT BLACKERBY LAND PARCEL, JUNEAU, ALASKA

Jillian A. Nicolazzo and Martin C. Larsen

Preliminary Interpretative Report 2024-7

2025
STATE OF ALASKA
DEPARTMENT OF NATURAL RESOURCES
DIVISION OF GEOLOGICAL & GEOPHYSICAL SURVEYS

STATE OF ALASKA
Mike Dunleavy, Governor

DEPARTMENT OF NATURAL RESOURCES
John Boyle, Commissioner

DIVISION OF GEOLOGICAL & GEOPHYSICAL SURVEYS
Melanie Werdon, State Geologist & Director

Publications produced by the Division of Geological & Geophysical Surveys are available to download from the DGGS website (dggs.alaska.gov). Publications on hard-copy or digital media can be examined or purchased in the Fairbanks office:

Alaska Division of Geological & Geophysical Surveys (DGGS)
3354 College Road | Fairbanks, Alaska 99709-3707
Phone: 907.451.5010 | Fax 907.451.5050
dggspubs@alaska.gov | dggs.alaska.gov

DGGS publications are also available at:

Alaska State Library, Historical
Collections & Talking Book Center
395 Whittier Street
Juneau, Alaska 99801

Alaska Resource Library and
Information Services (ARLIS)
3150 C Street, Suite 100
Anchorage, Alaska 99503

Suggested citation:
Nicolazzo, J.A., and Larsen, M.C., 2025, Mass movement potential at Blackerby land parcel, Juneau, Alaska: Alaska Division of Geological & Geophysical Surveys Preliminary Interpretive Report 2024-7, 17 p., 1 sheet, scale 1:4,000. https://doi.org/10.14509/31275

MASS MOVEMENT POTENTIAL AT BLACKERBY LAND PARCEL, JUNEAU, ALASKA

Jillian A. Nicolazzo[1] and Martin C. Larsen [1]

INTRODUCTION

The Alaska Division of Mining, Land and Water (DMLW) requested information from the Division of Geological & Geophysical Surveys (DGGS) regarding the slope stability of the Blackerby land parcel in Juneau, Alaska (fig. 1). Although the City and Borough of Juneau (CBJ) previously completed a landslide and avalanche hazard assessment of the Juneau area (Tetra Tech, 2022, fig. 1), the DMLW parcel is located roughly 5,000 feet (1,500 meters) north of that study area, and existing geologic information in the area is limited to maps from the 1970s. To assist with the analysis, DGGS collected and processed a new light detection and ranging (lidar) dataset (Zechmann and others, 2024), which we used to interpret the landscape and as a basis for analyses. Additionally, DGGS conducted a site visit on October 18, 2023, to assess the area for unstable slopes and look for evidence of landslide or debris flow activity. During the site visit, water was noted flowing through the parcel originating in the bedrock slope located to the northeast; therefore, this upslope area was included in the project's study area. These contributing watersheds determined the study area's extent (fig. 1). This report discusses the field investigation, describes the datasets used, and details our mapping, modeling, and analysis methods.

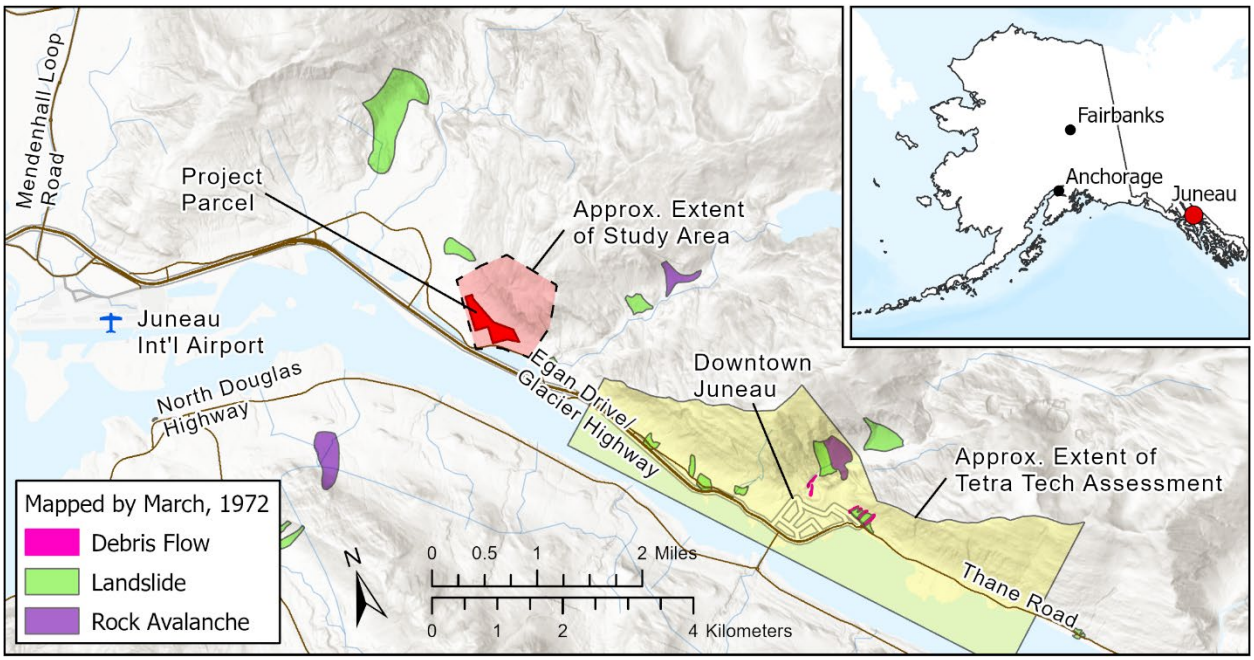

[1] Alaska Division of Geological & Geophysical Surveys, 3354 College Road, Fairbanks, AK 99709

Figure 1. Location map for the Blackerby land parcel (red polygon) and study area (dashed black polygon), also showing previously mapped landslides and the extent of the 2022 Tetra Tech Canada, Inc. landslide assessment.

METHODS

Existing Information

The best reference for landslides near the project parcel is a 1975 geologic map that identified two landslides: one approximately 1,900 feet (580 meters) south, and one approximately 2,200 feet (670 meters) north (Miller, 1975; fig. 2) of the parcel. No mass wasting deposits, or mass movements were mapped or identified within the parcel (Miller, 1975). There are numerous news articles that discuss landslides, debris flows, and other mass wasting events that have occurred in Juneau, including at least two that mention flooding, debris flows, and property damage resulting from the December 2020 storm (Alaska Coastal Rainforest Center, no date; KTOO News Department, 2020), but little information regarding this project's parcel. In 2022, Tetra Tech Canada Inc. completed a landslide and avalanche hazard assessment for the downtown area of Juneau (Tetra Tech, 2022), but their analysis did not include this project's parcel (fig. 1). The area around downtown Juneau has a history of landslide activity that has impacted lives and infrastructure. The devastating 1936 landslide affected downtown Juneau and claimed 15 lives (Canny, 2024). In addition, the 1975 geologic map identifies multiple mass-wasting deposits (landslide, debris flow and rockslide avalanche) throughout the area (fig. 1).

Geologic units mapped within the parcel consist of Holocene and Pleistocene glaciomarine deposits comprising diamicton (boulders, cobbles, sand, and silt), mollusks, and Foraminifera (Miller, 1975; fig. 2). Geologic units mapped upslope of the parcel include talus (Miller, 1975) and bedrock composed of chlorite schist, greenschist, phyllite, and slate (Ford and Brew, 1973; fig. 2).

DGGS reviewed existing lidar datasets from 2012 and 2013 (OCM Partners, 2024, and Watershed Sciences, Inc., 2013, respectively). The 2012 dataset included the parcel and the slopes above, but snow obscured the higher elevations, and the 2013 dataset did not include the higher elevations. Because of these limitations these datasets were not used, and new lidar was collected. We also reviewed available aerial imagery, but the dense vegetation and tree cover obscured the ground surface limiting its usefulness.

Lidar Acquisition and Processing

DGGS collected lidar for the study area on July 12, 2023, using a Riegl VUX1-LR22 laser scanner integrated with a global navigation satellite system (GNSS) and Northrop Grumman LN-200C inertial measurement unit (IMU). The data were processed in house and published as a separate raw data file that discusses the equipment used and data processing techniques (Zechmann and others, 2024). Zechmann and others (2024) used the point cloud to generate a digital terrain model (DTM) representing the bare earth elevations (excluding vegetation and buildings), and we derived rasters from the DTM for the slope stability analyses presented in this report. The DTM is a 20-cm (7.8-in) resolution, single-band, 32-bit GeoTIFF raster file.

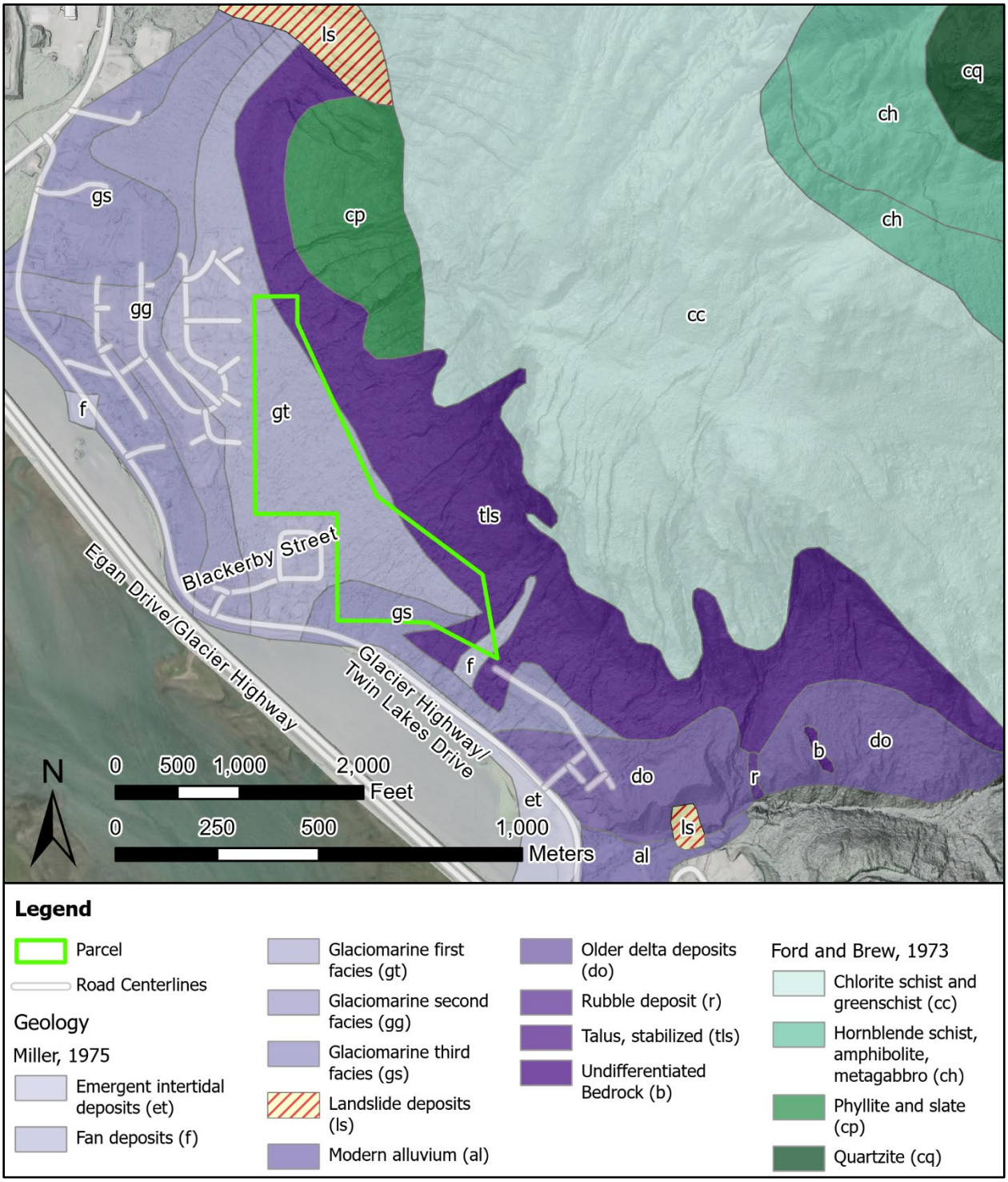

Figure 2. Geologic map (surficial mapping by Miller, 1975; bedrock mapping by Ford and Brew, 1973) displayed over a 20-cm DTM-derived, multi-directional hillshade raster (DTM by Zechmann and others, 2024).

Lidar Interpretation

DGGS followed landslide inventory mapping protocols described in Burns and Madin (2009) and Slaughter and others (2017). We used Esri's ArcGIS Pro software version 3.2.1 to derive hillshade, slope, and curvature raster files from the 2023 DTM (Zechmann and others, 2024). The topography within the parcel consists of gently west–southwest dipping slopes averaging 18 degrees with a standard deviation of 9.3 degrees (fig. 3). No landslide or debris flow deposits were identified within the parcel; however, several rockfall scarps are visible in the steep bedrock slopes above the parcel (fig. 4). We used Esri's Hydrology geoprocessing tools to identify drainages and potential debris flow channels (fig. 5).

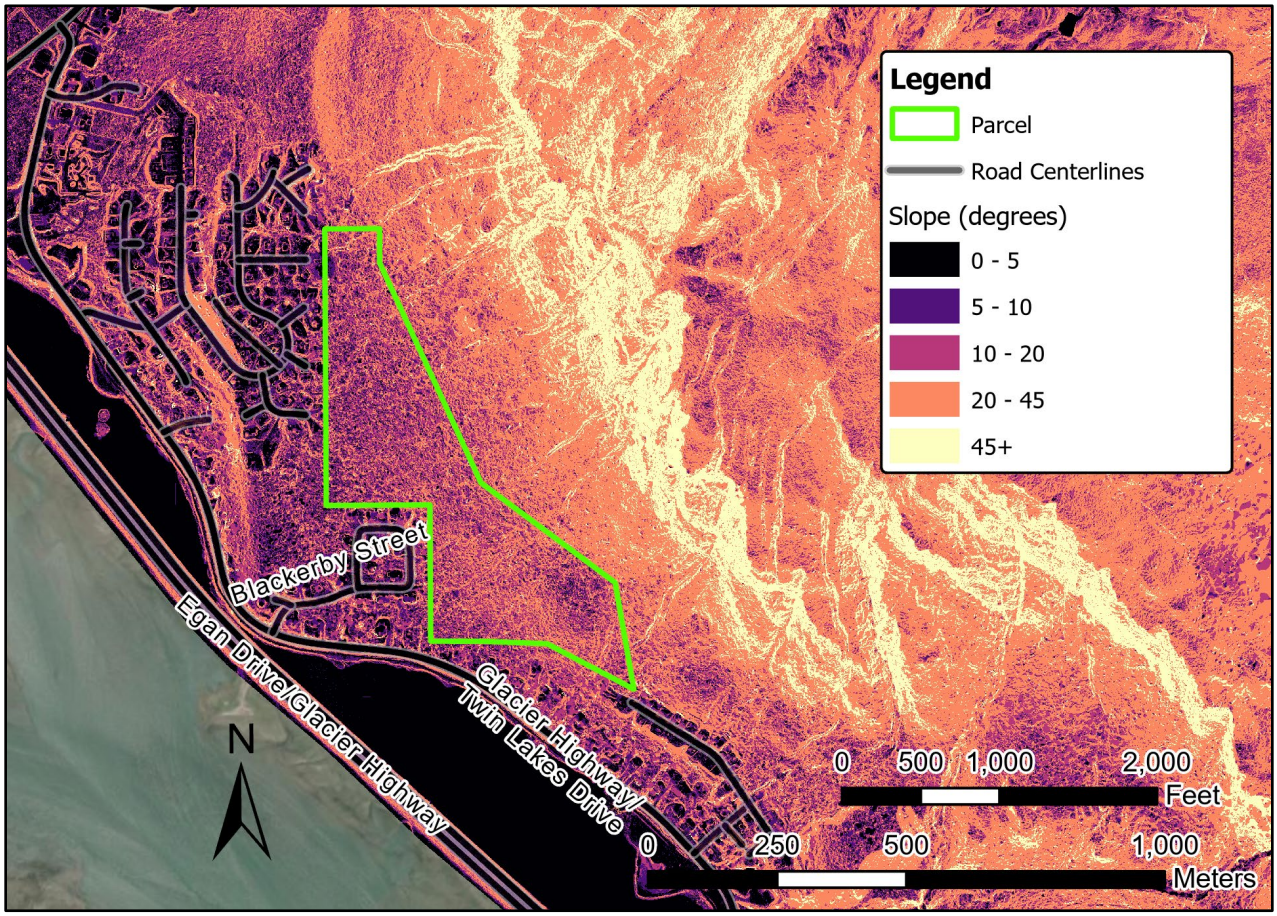

Figure 3. Slope raster derived from the 2023 DTM (Zechmann and others, 2024).

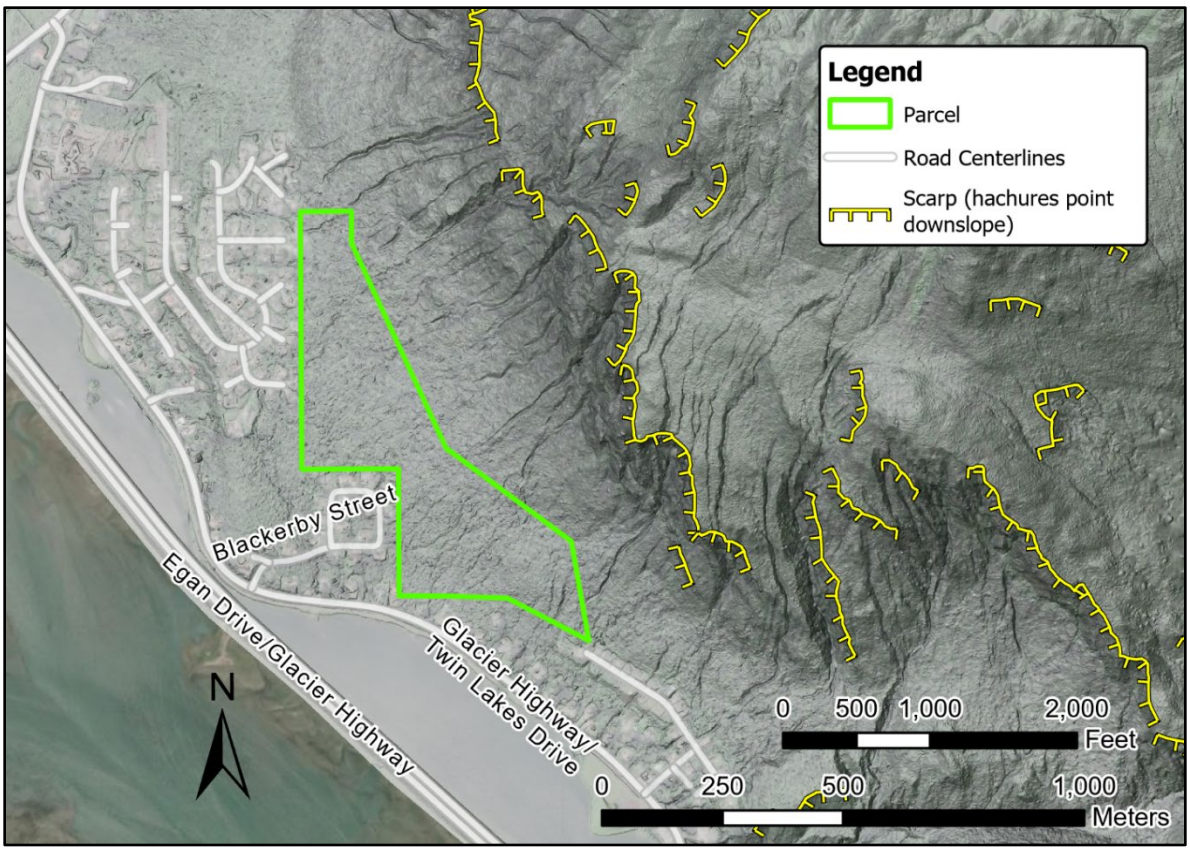

Figure 4. Scarps identified in the 2023 DTM (Zechmann and others, 2024) displayed on a partially transparent, multi-directional hillshade raster over the Alaska High Resolution Imagery (Maxar Products, 2020).

Site Visit

Two DGGS geologists conducted a site visit on October 18, 2023, to verify previously mapped soils and drainages and look for signs of landslides and debris flows not visible in lidar datasets or aerial imagery. We used Esri's Field Maps application to locate the parcel in the field, record GNSS field location points, and take notes and photographs. We accessed the parcel from Blackerby Street and walked both north and south along a hiking trail that is inside the eastern border of the parcel, roughly parallel to Egan Drive.

The parcel contains a mature forest that is heavily vegetated with ferns, moss, thick underbrush, and evergreens. Back-tilted, pistol-butted, or bent trees can indicate soil movement; none were observed within the parcel. Most of the drainages are narrow, shallow, and well channelized; however, at the southeastern tip of the parcel there is a wider and more deeply incised drainage (figs. 5 and 6) that is roughly 6 feet (2 meters) wide at the base and 20 feet (7 meters) deep. In general, exposed soils observed in the channelized drainages and stream beds consist of gray, poorly sorted, subrounded to rounded gravel and cobbles, with angular to subangular bedrock fragments, fine to coarse sand, and silt (fig. 6). We observed talus deposits at the base of the uphill slope. There was no evidence of landslide scarps, hummocky terrain, or debris flow deposits along the traverse; however, these features may exist in areas not traversed. Landslide features may also have been obscured by heavy vegetation or misidentified during the field investigation.

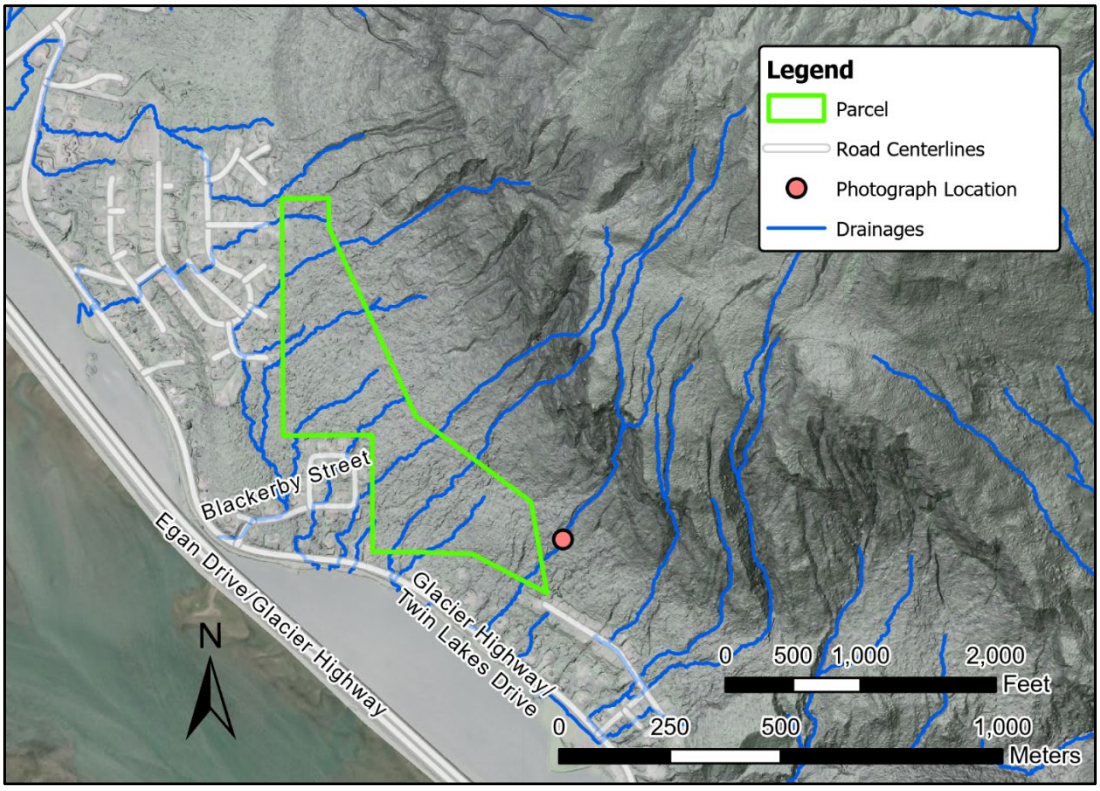

Figure 5. Drainages identified in the 2023 DTM (Zechmann and others, 2024) displayed on a partially transparent, lidar-derived, multi-directional hillshade raster over the Alaska High Resolution Imagery (Maxar Products, 2020). The red circle indicates the location of the photograph shown in figure 6.

Figure 6. Photograph showing the deeply incised drainage located at the southern tip of the parcel.

Shallow-Landslide Susceptibility Mapping

In this section, the word "landslide" generally refers to mass movements that have a distinct zone of weakness separating the slide materials from more stable underlying materials and includes translational and block landslides. It does not include debris flows, which are discussed in the next section, nor seismically induced movements that require site-specific information and are outside the scope of this project. The susceptibility map does not include ground failures such as liquefaction, lateral spread, or rockfall caused by seismic shaking.

Following the methodology of Burns and others (2012), DGGS developed a map of the study area showing slopes susceptible to shallow landslides. Shallow landslides occur in surficial soils, to a maximum depth of about 15 feet (4.5 meters) (Burns and others, 2012). This method combines areas of mapped shallow landslides with a calculated factor of safety (FOS). The result is a map that displays susceptibility as high, moderate, or low zones (map sheet 1).

Factor of Safety

The factor of safety (FOS) is the relationship between driving forces acting to move material downslope (e.g., gravity) and resisting forces acting to impede downslope movement (e.g., soil cohesion; Burns and others, 2012; eq. 1). Slopes with an FOS greater than 1.0 are theoretically stable (the shear resistance is greater than the shear stress), and those with an FOS less than 1.0 are theoretically unstable (the stress is greater than the resistance). Since soil and rock composition and their geotechnical properties vary across geologic units, a conservative approach is appropriate; therefore, an FOS less than 1.50 is generally considered to be unstable (Burns and others, 2012). For this project, FOS values less than 1.25 are classified as "highly" susceptible to failure, values from 1.25 to 1.50 are "moderately" susceptible to failure, and values equal to 1.50 or greater have low to no susceptibility to failure.

Equation 1. $$FOS = \frac{c'}{\gamma\, t \sin\alpha} + \frac{\tan\varphi'}{\tan\alpha} - \frac{m\,\gamma_w \tan\varphi'}{\gamma \tan\alpha}$$

Where:

c' = cohesion (effective)

φ' = angle of internal friction (effective)

γ = soil density (unit weight)

γ_w = groundwater density (unit weight)

t = depth to failure surface

m = groundwater depth ratio

α = slope angle

We relied on the identification of surficial deposits within the study area from Miller (1975) (fig. 2) to assign soil properties. This project did not include additional subsurface investigations or drilling operations, and there is little to no existing subsurface information. Soil properties (soil density/unit weight, cohesion, and phi angle) were assumed as follows.

Most of the parcel's surficial soils are of glaciomarine origin although a small portion is talus, and the area immediately upslope of the parcel was mapped as talus (Miller, 1975). Miller (1975) described the glaciomarine deposits as being "dense, till-like"; therefore, a higher phi angle and unit weight were assumed as compared to a looser, less dense soil (geotechdata.info, 2013; table 1). It was further assumed that any landslides that might occur would be shallow, or to the depth of bedrock. Where the bedrock depth is not known, we used a value of 15 feet (1.57 meters) (Burns and others, 2012). Based on the high average annual rainfall and the presence of several drainages, the groundwater depth ratio was assigned a value of 1 for all soils, which implies a fully saturated condition.

For this analysis, we treated bedrock as though it was a very dense, cohesive soil; the presence of talus deposits at the base of the slope indicates rockfall or raveling of the upslope bedrock has occurred. Modeling bedrock failure typically requires a detailed geotechnical engineering investigation to identify blocks that may be susceptible to releasing, site-specific information about the bedrock characteristics, and specialized software to model the bounce and roll of the blocks all of which are beyond the scope of this project. Modeling it as a soil and including it in this analysis allows us to estimate where the slope is steep enough that it might be susceptible to rockfall, and to show those areas on the map.

Table 1. Factor of safety input parameters. See equation 1 for explanation of variables.

Soil Unit (fig. 2)	Effective angle of internal friction φ'	Effective cohesion c'		Unit weight of soil γ		Depth of failure		Groundwater depth ratio
	degrees	lb/ft^2	kPa	lb/ft^3	kN/m^3	ft	m	
Glaciomarine first and second facies	40	0	0	132	20.7	15	4.57	1
Fan	28	0	0	104	16.3	15	4.57	1
Talus	38	0	0	130	20.4	15	4.57	1
Bedrock (all)	45	460	22	180	28.3	3	0.9	1

We calculated the FOS for each soil type for the full range of possible slopes, from 1.0 to 90.0 degrees, in 0.5-degree increments, noting slope angles corresponding to an FOS of 1.25 and 1.50 for each soil type (table 2). We used these threshold values to select areas with steeper slopes from the 2023 DTM-derived slope raster using ArcGIS Pro and mosaicked the resultant rasters into a single dataset.

Table 2. Critical slope values per soil unit designating sloping areas moderately (FOS < 1.50) and highly (FOS < 1.25) susceptible to failure.

Soil Unit (fig. 2)	Slope angle threshold for FOS < 1.25	Slope angle threshold for FOS < 1.50
	degrees	degrees
Glaciomarine first and second facies	20.0	17.0
Fan	10.0	8.5
Talus	18.0	15.5
Bedrock (all)	55	65

Buffers and Smoothing

Landslides tend to have a steep headscarp that may fail retrogressively, or a new landslide may form above the scarp due to the removal of resisting forces directly below and adjacent to the scarp (i.e., the material that had been holding it in place is no longer there). Burns and others (2012) state that flat areas near an existing headscarp are at higher risk of failure than the FOS calculations might indicate and recommend adding a buffer equal to 2 horizontal to 1 vertical (2H:1V) to known headscarps to account for this additional risk. The scarps we identified are not all headscarps but because they are in bedrock and may be prone to rockfall, we applied this buffer to all identified scarps. Bedrock was assumed to have a failure of depth of 3 feet (0.9 meters; table 1); therefore, the applied horizonal buffer was equal to 6 feet (1.8 meters).

Creating a slope map from high-resolution lidar can result in the false classification of small-scale, low-relief features that do not pose a significant hazard, such as ditches, retaining walls, and road cuts. Some of these man-made features were visible in the slope map of the neighborhoods adjacent to and downhill from the parcel. We used the Focal Statistics geoprocessing tool in ArcGIS Pro to smooth the raster, with a 16.5-foot (5-meter) square neighborhood. After several iterations of the tool, this setting seemed to effectively remove single pixel, or small isolated susceptibility "islands" from within a larger area of consistent susceptibility without compromising the accuracy of the analysis; however, it did not entirely remove the structures. Their presence does not affect the analysis, but, to reduce their visual influence on the map, we generated a buffer from the road polylines and manually adjusted the resulting polygon to include other man-made structures that were initially outside of the buffer (e.g., houses). We converted this adjusted polygon to a raster and used Esri's Raster Calculator tool to decrease the susceptibility value of the cells within this mask by one level of susceptibility. For example, cells that were previously classified as highly susceptible now display as moderate, and those that were classified as moderately susceptible now display as having low susceptibility.

Channelized Debris Flow Susceptibility Mapping

Debris flows are a form of mass movement characterized by a slurry of water, soils, rocks, trees, and other debris quickly moving down slope under the influence of gravity. They are often associated with large rain events and are among the most destructive and expensive geohazards that occur in the state (Division of Homeland Security & Emergency Management, 2023).

Burns and others (2022) describe a method to generate a map of slopes susceptible to channelized debris flows and include custom ArcGIS geoprocessing tools to simplify the process. This method models debris flow initiation potential, transport potential, and deposition extents to produce a map that displays debris flow susceptibility in high, moderate, or low zones. Because this project's study area does not contain previously or newly mapped debris flows, we used Burns and others' (2022) suggested values for modeling, recognizing that these values were developed for Oregon and may not perfectly match site conditions in Alaska. A future, more detailed investigation could use debris flows in the wider Juneau area to calibrate these model input values.

Initiation

Based on the protocol, we assigned susceptibility values of 1–4 corresponding to no, low, moderate, and high susceptibility, respectively, to a range of slope and curvature raster values (table 3). Slopes 55 degrees and greater were not included in the analysis since they are less likely to accumulate the colluvium (loose, unconsolidated sediment) necessary for channelized debris flow initiation (Burns and others, 2022). The curvature raster identifies topography that is concave or convex and indicates where water and colluvium might collect (in concave, negative values) or be dispersed (from convex, positive values).

Stream channels located during the site visit were used as a comparison to the curvature-based drainage network generated by the geoprocessing tools developed by Burns and others (2012). The tool then created distance buffers around the identified drainages: 300 feet (91 meters) for "low" susceptibility to initiation areas, which covers most of the parcel, and distances less than 300 feet (91 meters) for "moderate" and "high" susceptibility areas (Burns and others, 2012; table 3).

Table 3. Summary of values for debris flow initiation potential (Burns and others, 2022).

Assigned Value	Category	Slope (degrees)	Curvature	Distance to drainage	
			1/100 ft	ft	m
4	High	35 to < 55	≤ -0.4	≤ 100	≤ 30.5
3	Moderate	25 to ≤ 35	-0.4 to ≤ 0.3	100 to ≤ 200	30.5 to ≤ 61
2	Low	15 to ≤ 25	0.3 to ≤ 1.1	200 to ≤ 300	61 to ≤ 91.4
1	Very low to none	≤15	Greater than 1.1	Geater than 300	Geater than 91.4

The final initiation potential score is the sum of the slope, curvature, and distance buffer values, culminating in a single value (table 4).

Table 4. Final debris flow initiation susceptibility scores (Burns and others, 2022).

Score	Susceptibility Class
12	High
9 to 11	Moderate
6 to 8	Low
5 or less	Very low to none

Transport

Once a debris flow begins to move down a channel, certain conditions must exist for it to continue. Burns and others (2022) use channel gradient and confinement as the two primary criteria to define the transportation potential of a flowing channelized debris flow. Their tool divides the drainage network created in an earlier step (see Initiation) into 100-foot (30.5-meter) segments, which are used as the flow paths for transportation potential.

Channel gradient is the downhill slope of the channel, defined by the number of feet (meters) the channel drops per mile (kilometer) along its length. Steeper channel gradients are more likely to transport debris flows than shallower gradients, and debris is more likely to deposit where the gradient becomes shallower (Burns and others, 2022).

Channel confinement is defined as the ability of a channel to move laterally. The tool created by Burns and others (2022) transects the channel segments perpendicularly at 25-foot (8-meter) intervals that extend 100 feet (30.5 meters) to either side of the channel line, creating five transect lines per segment. Points are placed at 9-foot (3-meter) intervals along the transect lines and the elevation at each point is extracted from the DEM. The difference between the highest and lowest elevation values for each transect line is calculated, and the average of the differences for the five transect lines for each channel segment is calculated and assigned to that channel segment. This value defines the amount of confinement for that segment; a difference of 10 feet (3 meters) along the 100-foot (30.5-meter) segment indicates low confinement (the channel can more easily shift side to side), whereas a difference of 75 feet (23-meter) along the 100-foot (30.5-meter) segment indicates high confinement (the channel cannot easily shift laterally).

We used the values suggested by Burns and others (2022) for this project (table 5). The final channel transport susceptibility score is the sum of the confinement value of each segment and the channel gradient value (table 6).

Table 5. Summary of values for channel transport potential (Burns and others, 2022).

Assigned Value	Category	Confinement	Gradient
		vertical feet per 100-foot increment	degrees
4	High	40 and greater	15 and greater
3	Moderate	20 to < 40	7.5 to < 15
2	Low	10 to < 20	5 to < 7.5
1	Very low to none	≤10	≤ 5

Table 6. Final channel transport susceptibility scores (Burns and others, 2022).

Score	Susceptibility Class
8	High
6 and 7	Moderate
4 and 5	Low
Less than 4	Very low to none

Watershed

A watershed is the upslope area that contributes flow to a common outlet. The tool created by Burns and others (2022) generates watersheds using standard hydrography tools in ArcGIS Pro and applies user-defined pour points (outlets) and the transport channels created in an earlier step (see Transport). Initiation and transport susceptibility scores are joined to each watershed polygon and summed to create a final susceptibility score per watershed (Burns and others, 2022; table 7).

Table 7. Final susceptibility score per watershed (Burns and others, 2022).

Score	Susceptibility Class
8	High
6 and 7	Moderate
4 and 5	Low
Less than 4	Very low to none

Inundation/Deposition

Laharz is a computer model developed for the U.S. Geological Survey that simulates the behavior of volcanic mudflows, known as lahars, and was modified to include channelized debris flows (Schilling, 1998). Burns and others (2022) extend the Laharz model to include the ability for volumes to expand as they flow down channel.

Burns and others (2022) recommend modeling debris flows for three scenarios: typical, intermediate, and extreme. The "typical" scenario has a small to medium impact and a high relative reoccurrence interval; this event might occur every few years or decades. An "extreme" scenario has a large to extreme impact and a low relative reoccurrence interval; it might happen once per millennia or less frequently. Characteristics of an "intermediate" scenario fall between typical and extreme. Two input values are required for modeling each scenario: growth factor and maximum volume. Growth factor defines the erosion and entrainment of debris that add to the volume of a debris flow moving down channel. The maximum volume limits how large the debris flow can grow (Burns and others, 2022).

Input values for the typical scenario are selected and adjusted until the modeled inundation area overlaps and closely matches mapped debris flows in the area (Burns and others, 2022); however, there are no known debris flows in the study area to use for comparison. In their table 16, Burns and others (2022) provide corresponding values for the intermediate and extreme scenarios. We used these same input values (table 8) to model debris flows for this project (map sheet 1). A future, more detailed study could calibrate these values to the characteristics of known debris flows across the broader Juneau area.

Table 8. Input values for channelized debris flow inundation scenarios (Burns and others, 2022).

Scenario	Growth Factor		Maximum Volume	
	ft^3/ft^3	m^3/m^3	ft^3	m^3
Typical	0.105	0.032	1,236,013	35,000
Intermediate (not shown on map sheet)	0.353	0.100	1,977,621	56,000
Extreme	1.130	0.320	3,531,467	100,000

RESULTS

Landslide and Debris Flow Inventory

We did not identify any recent or historical landslides or debris flows within the study area. While inspecting the 2023 DTM (Zechmann and others, 2024), we identified several rockfall scarps upslope of the parcel at the top of steep drainages. These drainages contain angular bedrock and gravels and may be conduits for transporting debris from upslope.

Susceptibility Maps

Most of the parcel is of glaciomarine origin, which means the assumed soil properties across the parcel are the same. The slope angle across the property varies only slightly. Taken together, this consistency indicates the susceptibility to landslides across the parcel is similar, with little variation (map sheet 1). The FOS calculations suggest that slopes steeper than roughly 15–20 degrees are moderately susceptible to failure, and those steeper than approximately 20 degrees are highly susceptible to failure (table 2). The average slope across the parcel is 18.5 degrees (fig. 3), which indicates the parcel is, on average, moderately susceptible to movement. Nearly half (49 percent) of the parcel is categorized as low susceptibility, 12 percent as moderate susceptibility, and 39 percent as high susceptibility (table 9, map sheet 1). Generally, the southern half of the parcel has slightly steeper slopes than the northern half and therefore has higher landslide susceptibility. Mostly, the higher susceptibility is situated along the drainage slopes located at the southeastern area of the parcel. Throughout the rest of the parcel, the higher susceptibility areas are scattered, isolated, and are frequently bounded by areas of low susceptibility. The alluvial fan at the southern tip of the parcel (Miller, 1975; fig. 2) also has higher susceptibility due to its looser, transported soils (table 1). Other drainages with transported soils might also have a higher susceptibility than this report suggests due to the level of detail of the input geologic map.

Table 9. Landslide susceptibility results for the parcel.

Landslide Susceptibility	Percent of Parcel
	percent
Low	49
Moderate	12
High	39

In general, there is little to no risk of channelized debris flow initiation or inundation within the parcel (table 10, map sheet 1). The steep slopes above the parcel have moderate potential to initiate channelized debris flows and low to moderate transport potential. Inundation is expected to occur upslope from the parcel. The only exception to this is at the location of the largest drainage at the southeastern tip of the parcel. Currently, the parcel is drawn with a pointed end, but if it were to be redrawn to square-off that tip, extending it behind Greenwood Avenue, then inundation areas would overlap the parcel (map sheet 1).

Table 10. Debris flow susceptibility results in the parcel.

	Percent of Parcel Susceptible to Debris Flow Initiation	Percent of Parcel Susceptible to Debris Flow Inundation
	percent	percent
None/very low	100	100
Low	0	0
Moderate	0	0
High	0	0

INTENDED USE AND LIMITATIONS

This preliminary study identifies the relative slope failure hazard in the Blackerby parcel area and helps determine if additional studies are necessary before parcel planning begins. Limitations of the input data and modeling methods are such that the map is not suitable to answer site-specific, engineering, or legal questions. The map should only be used for community-scale purposes and is not intended to be viewed at scales other than the published map scale (1:4,000).

The landslide inventory and susceptibility maps were developed using the most reliable available data; however, some of the limitations include:

- The susceptibility maps presented here are heavily based on lidar data. Lidar-based mapping is a "snapshot" view of the landscape at the time the lidar dataset was collected and does not represent changes that may have occurred after it was collected. Limitations in lidar collection and processing also apply to these maps.
- Due to the obscuring vegetation cover in available aerial imagery, limited field verification, and reliance on lidar-based mapping, some landslides and debris flow deposits may have been misidentified or not mapped. Mapping may change as new information becomes available and as new landslides and debris flows occur.
- The Shallow Landslide Susceptibility Map was based on calculated factor of safety, which incorporates previously mapped soil types and limited field data. Depth to failure, depth to groundwater, and soil engineering properties were assumed based on our best judgment and with a conservative approach; however, local conditions may vary significantly from the values used to make this map.
- Because there are no mapped debris flows in the area, the Channelized Debris Flow Susceptibility map is based on an assumed "typical" event size that does not represent an actual, historical event that occurred in the area. The "extreme" event is scaled up from the assumed typical event.

CONCLUSION

The Division of Geological & Geophysical Surveys completed a preliminary hazard assessment for the Blackerby parcel for the Division of Mining, Land and Water by first

researching the known occurrences of landslides and debris flows in the area, collecting and processing new lidar data, estimating the relative susceptibility for both shallow landslides and channelized debris flows, and generating maps to show these susceptibilities. On average, the parcel is moderately susceptible to shallow landslides, with the area around the drainage at the southeastern end having a higher susceptibility, and it is not likely to be inundated by a debris flow.

Landslide susceptibility mapping and slope stability analyses are essential for producing high-quality hazard maps and providing information to planners who can use these data to implement guidelines and directions for local planning and development. The results of the slope stability analysis and resultant maps can assist planners to evaluate site conditions and determine if additional investigations and mitigation measures are needed to address the identified hazards in this area.

ACKNOWLEDGMENTS

Funding for this project was provided by the State of Alaska Division of Mining, Land and Water (Reimbursable Service Agreement- IPO 230001027). We would like to thank the Division of Mining, Land and Water staff, especially Colin Craven and Amund Rongstad, for providing this opportunity. J. Barrett Salisbury provided thoughtful comments, which improved the quality of this product.

REFERENCES

Alaska Coastal Rainforest Center, no date, Juneau climate report: Land, University of Alaska Southeast. [Accessed July 10, 2024] https://acrc.alaska.edu/juneau-climate-report/land.html

Burns, W.J., Franczyk, J.J., and Calhoun, N.C., 2022, Protocol for debris flow susceptibility mapping: Oregon Department of Geology and Mineral Industries Special Paper 53, 89 p. https://pubs.oregon.gov/dogami/sp/SP-53/p-SP-53.htm

Burns, W.J., and Madin, I.P., 2009, Protocol for inventory mapping of landslide deposits from light detection and ranging (lidar) imagery: Oregon Department of Geology and Mineral Industries Special Paper 42, 30 p. https://www.oregongeology.org/pubs/sp/p-SP-42.htm

Burns, W.J., Madin, I.P., and Mickelson, K.A., 2012, Protocol for shallow landslide susceptibility mapping: Oregon Department of Geology and Mineral Industries Special Paper 45, 32 p. https://pubs.oregon.gov/dogami/sp/p-SP-45.htm

Canny, Anna, 2024, Juneau's deadliest landslide tore through downtown like a 'mighty grinder'. Now it's a fading memory, Alaska Public Media. [Accessed August 19, 2024] https://alaskapublic.org/2024/01/16/juneaus-deadliest-landslide-tore-through-downtown-like-a-mighty-grinder-now-its-a-fading-memory/

Division of Homeland Security & Emergency Management, 2023, State of Alaska Hazard Mitigation Plan (SHMP): State of Alaska Hazard Mitigation Plan, 274 p. https://ready.alaska.gov/Mitigation/SHMP

Ford, A.B., and Brew, D.A., 1973, Preliminary geologic and metamorphic-isograd map of the Juneau B-2 Quadrangle, Alaska: U.S. Geological Survey Miscellaneous Field Studies Map 527, 1 sheet, scale 1:31,680. https://dggs.alaska.gov/pubs/id/13250

Geotech data, 2013, Geotechnical parameters. [Accessed October 2023] http://www.geotechdata.info/parameter/

KTOO News Department, 2020, Record rain brings floods and mudslides to Juneau, KTOO. [Accessed July 10, 2024] https://www.ktoo.org/2020/12/02/record-rain-brings-floods-and-mudslides-to-juneau/

Maxar Products, 2020, Alaska statewide high-resolution imagery (50cm) RGB map image layer. [Accessed 2023 and 2024] https://geoportal.alaska.gov/portal/home/item.html?id=d462231cc1454e1abb2dccd9a709a476

Miller, R.D., 1975, Surficial geologic map of the Juneau urban area and vicinity, Alaska: U.S. Geological Survey Miscellaneous Investigations Series Map 885, 1 sheet, scale 1:48,000. https://dggs.alaska.gov/pubs/id/12956

OCM Partners, 2024, 2012 USGS Lidar: Juneau (Alaska): National Oceanic and Atmospheric Administration National Centers for Environmental Information. https://www.fisheries.noaa.gov/inport/item/49625.

Schilling, S.P., 1998, LAHARZ; GIS programs for automated mapping of lahar-inundation hazard zones: U.S. Geological Survey Open-File Report 98-638, 80 p. https://doi.org/10.3133/ofr98638

Slaughter, S.L., Burns, W.J., Mickelson, K.A., Jacobacci, K.E., Biel, Alyssa, and Contreras, T.A., 2017, Protocol for landslide inventory mapping from lidar data in Washington State: Washington Geological Survey Bulletin 82, 27 p., text, with 2 accompanying ESRI file geodatabases and 1 Microsoft Excel file. http://www.dnr.wa.gov/Publications/ger_b82_landslide_inventory_mapping_protocol.zip

Tetra Tech, 2022, Downtown Juneau landslide and avalanche hazard assessment, presented to the City and Borough of Juneau, 289 p. https://juneau.org/wp-content/uploads/2022/09/April-27-2022-full-Downtown-Juneau-Landslide-and-Avalanche-Hazard-Assessment-IFUwebsize.pdf

Watershed Sciences, Inc., 2013, Juneau LiDAR and orthophotos technical data report-final delivery. https://dggs.alaska.gov/pubs/id/25239

Zechmann, J.M, Larsen, M.C., and Wikstrom Jones, K.M., 2024, Lidar-derived elevation data for Blackerby parcel, Juneau, Southeast, Alaska, collected July 12, 2023: Alaska Division of Geological & Geophysical Surveys Raw Data File 2024-8, 8 p. https://doi.org/10.14509/31161